Tungsten black absorber for solar light with wide angular operation range

Eden Rephaeli[1,a)] and Shanhui Fan[2]
[1]*Department of Applied Physics, Stanford University, Stanford, California 94305, USA*
[2]*Department of Electrical Engineering, Stanford University, Stanford, California 94305, USA*

(Received 18 March 2008; accepted 29 April 2008; published online 29 May 2008)

Using three-dimensional finite-difference time-domain simulations, we designed a structured tungsten slab with subwavelength periodicity that displays near-complete absorptivity throughout the entire solar spectrum over a wide angular range. The structure consists of a square lattice array of pyramids. The parameters of the pyramids are chosen to provide the optimal impedance matching between free space and tungsten, while the period is chosen to be subwavelength in order to generate absorption over an ultrabroad band of wavelengths. © *2008 American Institute of Physics*. [DOI: 10.1063/1.2936997]

In solar-thermal applications, one aims to convert sunlight to heat. The key component then is a solar absorber that provides strong absorption of sunlight. Ideally, such an absorber needs to operate over the entire solar bandwidth. Moreover, since many of these applications require concentrated sunlight, and even direct sun light has a large diffusive component, it is important to design absorber that operates over a wide range of angles.

Previous designs of solar absorbers include the use of Cermet[1,2] films (MgO–Au, Cr_2O_3–Cr), low-density carbon nanotube arrays,[3] Si,[4] and metallodielectric photonic crystals.[5] In this letter, we focus on the design of a solar absorber based upon tungsten, a material with a high melting point, since many solar thermal applications, especially solar thermal photovolatics,[6,7] require absorbers that can withstand high temperatures.

While there is significant amount of optical loss inside tungsten, a tungsten slab by itself is not a good absorber. Figure 1(a) shows the experimentally determined real and imaginary part of the tungsten dielectric constant, as taken from Ref. 8. Notice that the imaginary part of the tungsten dielectric constant is comparable to its real part in orders of magnitude, thus a wave propagating inside the tungsten would be completely absorbed within a few wavelengths of propagation distance. However, a semi-infinite slab of tungsten has an absorptivity [Fig. 1(b)] that is less than 50%. The rest of the incident power is reflected due to the impedance mismatch between tungsten and free space.

To design an efficient absorber, it is therefore essential to provide an impedance matching mechanism between free space and tungsten. Previously, it has been shown that highly efficient antireflection structures can be designed with the use of tapered subwavelength gratings[9–14] (SWG), where light is efficiently transmitted through the grating. Here we show that in tungsten, the use of tapered SWG allows one to create a highly efficient light absorbing structure, where the incident light is absorbed within the grating structure. Our design, shown in Fig. 2(a), consists of a square lattice array of tungsten pyramids with a 250 nm period in both transverse dimensions, and a height of 500 nm.

To simulate the structure shown in Fig. 2(a), we used a three-dimensional finite-difference time-domain method.[15]

To describe the effect of material dispersion and absorption in the time-domain simulation, the experimentally determined permittivity data of tungsten was fitted using the complex-conjugate pole-residue pairs method.[16] In this method, the complex permittivity is expressed as the sum of first-order complex-conjugate poles,

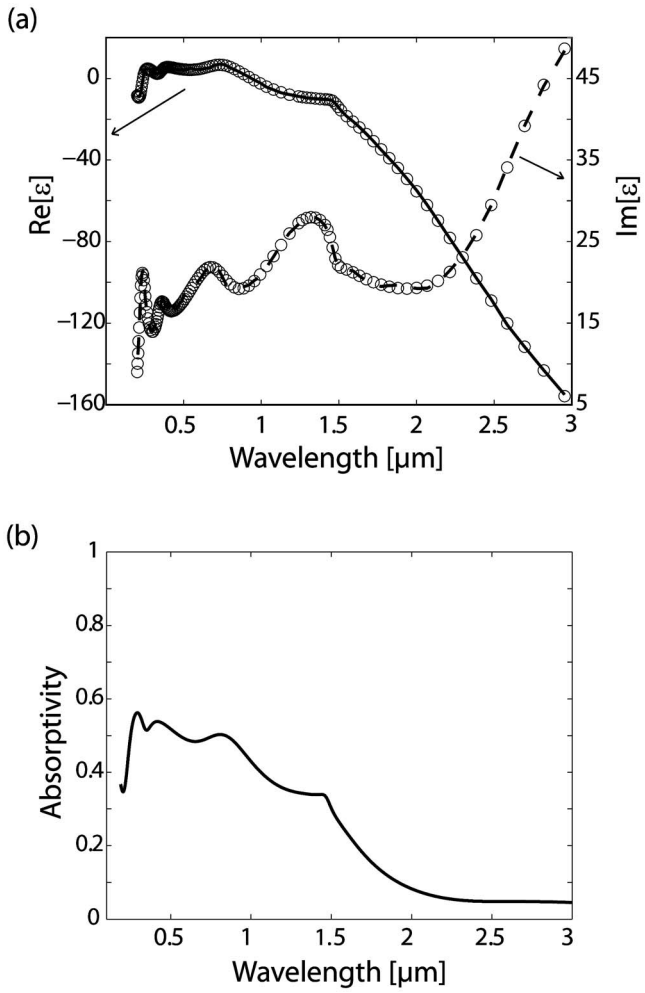

FIG. 1. (a) Real and imaginary parts of relative permittivity ε for tungsten. The circles represent experimental data from Ref. 8. The lines were fitted using the complex-conjugate pole-residue pairs with parameters given in Table I. (b) Absorptivity at normal incidence of semi-infinite tungsten slab.

a)Electronic mail: edenr@stanford.edu.

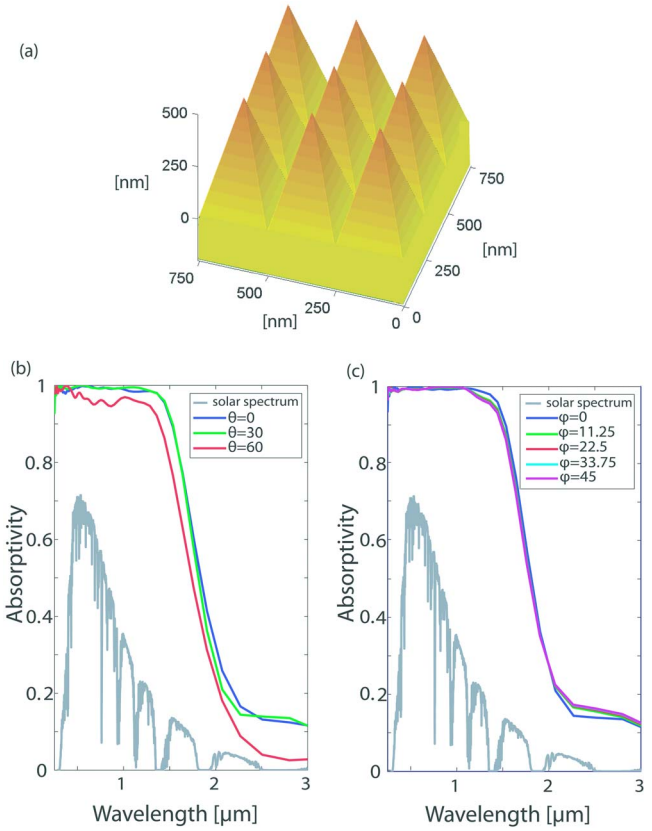

FIG. 2. (Color online) (a) Illustration of the tungsten pyramid structure with nine unit cells showing. (b) Simulated absorptivity for various polar angles of incidence. (c) Simulated absorptivity for $\theta=30°$ and various azimuthal angles. In both (b) and (c), the gray curve is the AM1.5 solar irradiance spectrum.

$$\varepsilon(\omega)=\varepsilon_0\left(\varepsilon_\infty+\sum_p\frac{c_p}{j\omega-a_p}+\sum_p\frac{c_p^*}{j\omega-a_p^*}\right), \tag{1}$$

where ε_0 is the dielectric constant of vacuum, $\varepsilon_\infty=1$. Using a nonlinear least squares fit, we obtained the coefficients c's and a's. These parameters are summarized in Table I. As can be seen in Fig. 1(a), the fit with these parameters is excellent over the entire wavelength range extending from 0.2 to 3 μm.

In time-domain simulation, each pole is described by an auxiliary differential equation with its own dynamic variables.[16] Also, to calculate the absorptivity of the structure at an oblique incidence angle, we implemented a field transformation algorithm,[17,18] which allows simulation of broadband responses for a single angle of incidence when enforcing periodic boundary conditions. The field transformation algorithm was combined with the complex-conjugate pole-residue pairs method in our simulation.

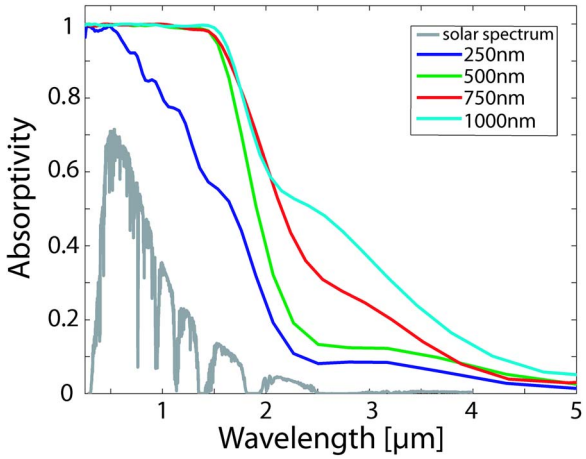

FIG. 3. (Color online) Simulated absorptivity for normal incidence ($\theta=0°$), for a structure with 250 nm period and with varying pyramid heights. The gray curve is the AM1.5 solar irradiance spectrum

In Fig. 2(b), the absorptivity of the pyramid structure is plotted for $\theta=0°$, 30°, and 60° with φ fixed at 0° [Fig. 2(b)], and for varying φ (0°, 11.25°, 22.5°, 33.75°, and 45°), with θ fixed at 30° [Fig. 2(c)]. θ and φ are the polar and azimuthal angles in a spherical coordinate system, respectively, where $\varphi=0°$ corresponds to directions that projects onto the [1 0] direction of the lattice. In Figs. 2(b) and 2(c), only the zeroth order spatial reflection coefficient was used to determine absorptivity. We have checked that all other propagating orders carry negligible energy. It can be seen that the absorptivity is practically unity (99.4% at 500 nm for normal incidence) for all solar wavelengths and varies only slightly for nonzero polar and azimuthal angles. In fact, we have checked that the absorber is virtually black for all angles of interest and is thus highly efficient.

Below we comment on some of the design considerations for such a tungsten solar absorber. The absorbing characteristics are strongly influenced by the height of the pyramid, as well as the periodicity. Increasing the height of the pyramid results in a longer and hence more gradual transition region from free space to tungsten, and in general improves the absorption characteristics. We have found through simulation that increasing the height in general leads to a broader absorption spectrum. In Fig. 3, it can be seen that for a height of 250 nm, there exists a very narrow plateau of unity absorptivity (around $\lambda=500$ nm) followed by a gradual linear decrease as wavelength increases. When the height is increased to 500 nm, a wide plateau is formed, with a rela-

TABLE I. Parameters for a fit of tungsten's relative permittivity with complex-conjugate pole-residue pairs.

Parameters	Values (eV)
(c_1,a_1)	$(1.686\times10^1+j\times4.196\times10^3,-7.520\times10^{-2}+j\times1.327\times10^{-3})$
(c_2,a_2)	$(1.693-j\times4.883\times10^{-1},-2.846\times10^{-1}+j\times1.676)$
(c_3,a_3)	$(-1.129\times10^1+j\times7.280\times10^2,-3.793\times10^{-1}+j\times1.988\times10^{-2})$
(c_4,a_4)	$(-3.877+j\times9.868,-6.869\times10^{-1}-j\times5.438)$
(c_5,a_5)	$(-1.984\times10^{-1}+j\times2.713,-8.871\times10^{-2}-j\times4.147\times10^{-1})$
(c_6,a_6)	$(-1.083+j\times1.442,-3.977\times10^{-1}-j\times3.608)$
(c_7,a_7)	$(1.095\times10^1+j\times4.196\times10^3,-2.893\times10^{-2}-j\times4.713\times10^{-3})$
(c_8,a_8)	$(7.066\times10^{-1}-j\times1.064,-1.326\times10^{-1}+j\times9.067\times10^{-1})$

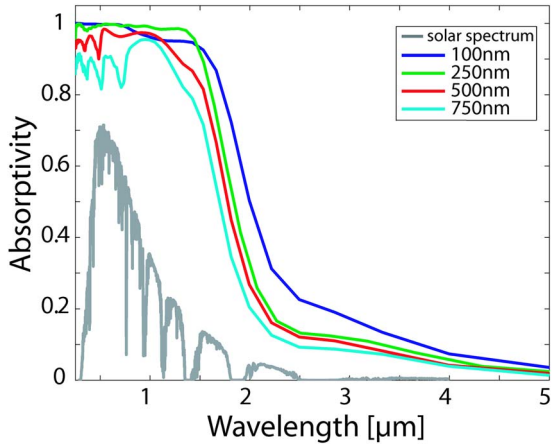

FIG. 4. (Color online) Simulated absorptivity at normal incidence ($\theta=0°$), for a structure with pyramid height of 500 nm, and varying periods. The gray curve is the AM1.5 solar irradiance spectrum.

tively sharp transition from unity to low absorptivity around 2 μm. Thus, such a height is sufficient to provide an effective impedance matching between air and tungsten, and the use of such structure greatly improves the absorption characteristics over a bare tungsten slab. [Fig. 1(b)]. Further increase of the height of the pyramid leads a more gradual slope in the longer wavelength range beyond 2 μm, without significantly affecting the absorptivity below 2 μm.

The absorption characteristics of our structure are also strongly influenced by its period. In the design, we chose the period to be 250 nm, which is smaller than most of wavelengths in the solar spectrum. This choice of a subwavelength period is critical, as can be seen from a sequence of simulations in Fig. 4, where we fix the height of the pyramid at 500 nm and vary the periodicity. Within the solar spectrum, very little difference is observed between two structures with periods of 100 and 250 nm. However, dips in the absorption plateau are observed when the period is increased beyond 250 nm, in addition to a generally lower absorptivity for all wavelengths. For light normally incident upon the structure, these dips occur at $\omega/c=|\mathbf{G}|$, where ω is the angular frequency, c is the speed of light in vacuum, and $\mathbf{G}$ is a reciprocal lattice vector of the structure.[19] For a periodicity of 500 nm, the first two dips are clearly present, corresponding to $\lambda=\lambda_p, \lambda_p/\sqrt{2}$, (where $\lambda_p=500$ nm). When increasing the periodicity to 750 nm, we see the first three Bragg peaks, corresponding to $\lambda=\lambda_p, \lambda_p/\sqrt{2}, \lambda_p/2$, (where $\lambda_p=750$ nm). The above peaks are detrimental to the absorber's efficiency since they occur around the peak of Blackbody power. Thus the use of a subwavelength period is critical to create broad band absorption in these structures.

In summary, this letter presents a design for a black absorber consisting of a periodic array of tungsten pyramids. Such an absorber could have important applications in solar thermal photovoltaics,[6] where a black absorber, displaying extremely high absorptivity for all solar wavelengths and incidence angles, can result in high energy conversion efficiencies. We have shown that a pyramid tapering solves the impedance mismatch problem between free space and a tungsten slab. In addition, we explored the implication of variation of design parameters, specifically the height and periodicity of the pyramids. It was shown that both the periodicity and height of the pyramids play a role in determining the structure's absorptive characteristics, and as such they were carefully chosen so as to optimize the structure's absorptivity.

[1] J. C. C. Fan and P. M. Zavracky, Appl. Phys. Lett. **29**, 478 (1976).
[2] J. C. C. Fan and S. A. Spura, Appl. Phys. Lett. **30**, 511 (1977).
[3] Z. P. Yang, L. Ci, J. A. Bur, S. Y. Lin, and P. M. Ajayan, Nano Lett. **8**, 446 (2008).
[4] C. M. Hsieh, J. Y. Chyan, W. C. Hsu, and J. A. Yeh, in Proceedings of IEEE/LEOS International Conference Optical MEMS Nanophotonics, 2007 (unpublished), p. 185.
[5] G. Veronis, R. W. Dutton, and S. Fan, J. Appl. Phys. **97**, 093104 (2005).
[6] N. P. Harder and P. Wurfel, Semicond. Sci. Technol. **18**, S151 (2003).
[7] S. Y. Lin, J. Moreno, and J. G. Fleming, Appl. Phys. Lett. **83**, 380 (2003).
[8] E. D. Palik, *Handbook of Optical Constants of Solids* (Academic, New York, 1985).
[9] Y. Kanamori, M. Ishimori, and K. Hane, IEEE Photonics Technol. Lett. **14**, 1064 (2002).
[10] Y. C. Kim and Y. R. Do, Opt. Express **13**, 1598 (2005).
[11] A. Gombert, W. Glaubitt, K. Rose, J. Dreibholz, B. Blasi, A. Heinzel, D. Sporn, W. Doll, and V. Wittwer, Thin Solid Films **351**, 73 (1999).
[12] Z. Yu, H. Gao, W. Wu, and H. Ge, J. Vac. Sci. Technol. B **21**, 2874 (2003).
[13] Y. Kanamori, K. Hane, H. Sai, and H. Yugami, Appl. Phys. Lett. **78**, 142 (2001).
[14] S. J. Wilson and M. C. Hutley, Opt. Acta **29**, 993 (1982).
[15] K. Yee, IEEE Trans. Antennas Propag. **14**, 302 (1966).
[16] M. Han, R. W. Dutton, and S. Fan, IEEE Microw. Wirel. Compon. Lett. **16**, 119 (2006).
[17] A. Taflove and S. C. Hagness, *Computational Electrodynamics: The Finite-Difference Time-Domain Method* (Artech House, Boston, 2000), pp. 603–610.
[18] J. A. Roden, S. D. Gedney, M. P. Kesler, J. G. Maloney, and P. H. Harms, IEEE Trans. Microwave Theory Tech. **46**, 420 (1998).
[19] D. L. C. Chan, M. Soljacic, and J. D. Joannopoulos, Opt. Express **14**, 8785 (2006).